JOURNAL OF CHEMICAL INFORMATION AND MODELING

Article

pubs.acs.org/jcim

Predicted Structures for Kappa Opioid G-Protein Coupled Receptor Bound to Selective Agonists

Quanjie Li,[†,‡] Soo-Kyung Kim,[†] William A. Goddard III,[*,†] Guangju Chen,[‡] and Hongwei Tan[‡]

[†]Materials and Process Simulation Center (MC-139-74), California Institute of Technology, Pasadena, California 91125, United States

[‡]College of Chemistry, Beijing Normal University, Beijing, 100875, People's Republic of China

Supporting Information

ABSTRACT: Human kappa opioid receptor (κ-OR), a G protein-coupled receptor (GPCR), has been identified as a drug target for treatment of such human disorders as pain perception, neuroendocrine physiology, affective behavior, and cognition. In order to find more selective and active agonists, one would like to do structure based drug design. Indeed, there is an X-ray structure for an antagonist bound to κ-OR, but structures for activated GPCRs are quite different from those for the inactive GPCRs. Here we predict the ensemble of 24 low-energy structures of human kappa opioid receptor (κ-OR), obtained by application of the GEnSeMBLE (GPCR Ensemble of Structures in Membrane Bilayer Environment) complete sampling method, which evaluates 13 trillion combinations of tilt and rotation angles for κ-OR to select the best 24. To validate these structures, we used the DarwinDock complete sampling method to predict the binding sites for five known agonists (ethylketocyclazocine, bremazocine, pentazocine, nalorphine, and morphine) bound to all 24 κ-OR conformations. We find that some agonists bind selectively to receptor conformations that lack the salt bridge between transmembrane domains 3 and 6 as expected for active conformations. These 3D structures for κ-OR provide a structural basis for understanding ligand binding and activation of κ-OR, which should be useful for guiding subtype specific drug design.

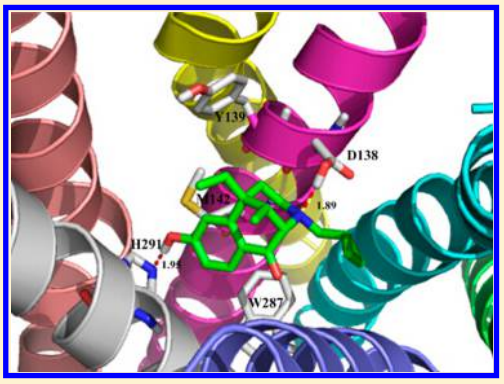

1.0. INTRODUCTION

Opioid receptors belong to the Class A (rhodopsin-like) subfamily of G protein-coupled receptors (GPCRs) with a common seven transmembrane (TM) helical architecture.[1,2] Four subtypes of opioid receptors, μ, δ, κ, and the nociceptin/orphanin FQ peptide receptor, are known, all of which play a significant role in physiological functions.[3−6] On the basis of studies of the κ-type prototypic agonist ketocyclazocine,[7] human kappa opioid receptor (κ-OR) was identified as an excellent drug target for the treatment of such human disorders as pain perception, neuroendocrine physiology, affective behavior, and cognition.[8] Several selective κ-OR agonists and antagonists have been developed as potential antidepressants, anxiolytic, and antiaddiction medications.[9] However, one would like to modify these ligands to achieve improved activity and selectivity.

In order to enable structure-based drug design, we need the structures for stable ligand/κ-OR structures. Indeed the crystal structure of the human κ-OR bound to the selective antagonist JDTic is available (PDB ID code 4DJH).[6] The ligand−receptor interaction provides important molecular details for κ-OR subtype selectivity and ligand binding. Unfortunately the X-ray structure of an antagonist bound to κ-OR is not sufficient for designing a new agonist. This is because GPCRs exhibit significant differences between the inactive and active states.[10−19] The activation of GPCRs is facilitated by their remarkable conformational flexibility, enabling the formation of multiple distinct conformations that can influence function.[13] This conformational flexibility poses considerable complexity to drug design, since it requires the knowledge of various conformational states to design a drug to shut down or enrich a particular active state of the receptor.[13,16−18,20] Thus, one cannot just consider one protein configuration, say from an X-ray structure.

To solve this problem of obtaining the ensemble of energetically favorable conformations available to play a role in multiple GPCR-mediated pathways, we have been developing the GEnSeMBLE (GPCR Ensemble of Structures in Membrane bilayer Environment) complete sampling method,[14,15,21,22] which has been successfully applied to predicting the structures for adenosine A_3,[16] cannabinoid CB1,[13] chemokine CCR5,[18,19] Glucagon-like peptide 1,[23] olfactory OR1G1,[17] and bitter taste Tas2R38[24] GPCRs. Here we apply GEnSeMBLE to predict the ensemble of 24 low energy structures of κ-OR. Within this ensemble we find 18 conformations with strong 3−6 coupling (potential inactive conformations) and 6 without such couplings (potential active conformations). We report here the hydrogen bond networks for the interhelical contacts to identify conformational switches that may lead to activation of the GPCRs.

Received: August 29, 2014
Published: February 2, 2015

DOI: 10.1021/ci500523z
J. Chem. Inf. Model. 2015, 55, 614−627

To validate these predicted conformations for κ-OR, we predicted the binding site and binding energy for five known agonists (ethylketocyclazocine, bremazocine, pentazocine, nalorphine, and morphine) to the top 24 structures using the DarwinDock complete sampling method. The predicted binding affinities for each ligand correlate well with the experimental data. On the basis of these structures of κ-OR, we propose a structural basis for the activation mechanism that may be useful for designing subtype specific ligands.

2.0. METHODS

2.1. GEnSeMBLE Method for Predicting Protein Structures. We predicted the ensemble of low energy GPCR structures using the GEnSeMBLE Complete Sampling method.[14,15,21,22] GEnSeMBLE identifies the TM domains based on multiple sequence alignments, then selects the shape of each helix based on the force field or on homology to known structures, and then considers a complete set (~13 trillion combinations) of rigid rotations and tilting of the helices, to select ~24 that are sufficiently stable to play a role in binding of ligands and activation. These procedures are described in more detail in the Supporting Information Text S1. All simulations used the Dreiding force field.[25]

2.1.1. TM Domains. GEnSeMBLE uses the PredicTM method to predict TM regions based on a multiple sequence alignment of GPCRs and using the octanol hydrophobicity scale.[26] These predicted regions are extended to include the entire section with α-helical character based on a consensus of secondary structure server predictions. However, because the crystal structure of κ-OR is available (PDB ID code 4DJH),[6] we instead used the helical sequence from the X-ray to define the seven TM regions, and we used the structure of each helix to define the rigid shape to be rotated.

GEnSeMBLE next considers several templates for similar proteins using structures from X-ray or previous computations. However, since the X-ray structure was available, we used the crystal structure itself as the template.

2.1.2. BiHelix. The BiHelix method[21] considers 12 helix rotation angles from $\eta = 0°$ to 360° for each of the 7 helices, leading to $(12)^7 = 35$ million combinations for which we estimate the energies using the BiHelix approximation. Thus, for each of the 12 interacting pairs of helices, we optimize side chain conformations using SCREAM (Side Chain Rotamer Excitation Analysis Method)[27] followed by 10 steps of conjugate gradient minimization to remove bad contacts. These pairwise energies are then used to evaluate the energies of all 35 million combinations, from which the 1000 lowest energy combinations are selected for the next step.[21]

2.1.3. ComBiHelix. In the ComBiHelix step the top 1000 conformations from BiHelix are built into full 7-helix bundles, for each of which the side chains are optimized with SCREAM followed by 10-steps of conjugate gradient minimization to remove bad contacts. We then selected the lowest energy conformation for the next step. This conformation is the same as in the X-ray structure, validating this procedure and the energy scoring.

2.1.4. SuperBiHelix. The SuperBiHelix method[22] starts with the optimum combinations of rotations from ComBiHelix and considers a systematic variation of tilt angle (θ), sweep angle (φ), and rotation angle (η) for each of the 7 helices (13 trillion total combinations) for which each energy is estimated with the SuperBiHelix procedure based on the pairwise interaction energies of all 12 pairs of interacting helices (after applying SCREAM and 10-steps of minimization). From these 13 trillion combinations we selected the best 2000 conformations for the next step.[15,22]

2.1.5. SuperComBiHelix. In the SuperComBiHelix step, we took the top 2000 conformations from SuperBiHelix, built each into full 7-helix bundles, for each of which the side chains were optimized with SCREAM followed by 10 steps of conjugate gradient minimization to remove bad contacts. From this ComBiHelix procedure we selected the lowest 24 conformations for ligand docking. The lowest energy of these 24 is the same conformation as in the X-ray structure, validating this procedure and the energy scoring.

2.1.6. Energy Scoring. In steps 4 and 6 we evaluate the total energy in four different ways. Two use the total energy of the 7-helix bundle while two use only the interaction energies between the helices. For each of these analyses we use two charge models: one uses standard charges which have a charge of −1.0 for D and E and a charge of +1.0 for R and K. The other neutralizes each amino acid by transferring the proton within a salt bridge or by adding or subtracting a proton for other cases. The 7-helix bundles are ranked by each of these 4 energies and then finally ordered by the average rank. This procedure has been validated for X-ray structures where this procedure always selects the X-ray combination of rotations from the top 10 of 35 million conformations in step 3 and the X-ray combination of tilts and rotations from top 24 of the 13 trillion in step 5, as was found for κ-OR.

2.2. DarwinDock Method for Predicting Ligand–Protein Structures. To predict the optimum ligand binding site to each of the 24 protein conformations from the GEnSeMBLE procedure, we used the DarwinDock method, which has previously been used to predict ligand−protein structures for many GPCRs.[13,16−18,23,24]

2.2.1. Selecting Ligand Conformations. Starting from the X-ray structure of the ligand, we sampled the torsion angles of all rotatable bonds to generate multiple conformations for each ligand. These were minimized using Maestro with 10 to 20 ligand conformations selected by energy and diversity. The charges on the ligands were Mulliken charges from density functional theory (B3LYP with the 6-311G** basis set).

2.2.2. Scanning the Receptor for Potential Binding Regions. For each of the 24 protein conformations, the whole protein was alanized (replacing the 6 hydrophobic residues, I, L, V, F, Y, and W with A). Then for each of the 10−20 ligand conformations, we scanned for potential binding regions with no assumption about the binding site. The entire molecular surface was mapped with spheres representing the empty volume of the protein. These spheres were partitioned using the BoxSpheres.pl script to generate 10 Å cubic boxes for each protein conformation. This led to a minimum of 73 boxes for WT13 and a maximum of 83 for WT24. We then used DOCK4.0[28] to generate 1000 poses for each of these 73−83 regions and selected the most promising three or four putative binding regions for docking.

2.2.3. DarwinDock. For each of the 24 protein conformations and each of the 10−20 ligand conformations, we generated iteratively ~50 000 poses spanning the putative binding regions of the bulky residue-alanized protein. These poses were generated in increments of 5000 and clustered into Voronoi families based on RMSD until <2% new families are generated. The family heads were scored using the Dreiding force field,[25] and the top10% by total energy were selected. Then we calculated the binding energy of all the members of these top 10% of families and selected the lowest 100 poses for further

DOI: 10.1021/ci500523z
J. Chem. Inf. Model. 2015, 55, 614−627

Table 1. Θ, φ, and η Values for the Top 24 κ-OR Conformations Generated from SuperCombiHelix

			θ							φ						η						
TM1	TM2	TM3	TM4	TM5	TM6	TM7	TM1	TM2	TM3	TM4	TM5	TM6	TM7	TM1	TM2	TM3	TM4	TM5	TM6	TM7	RMSD	RankCNti
0	*0*	*0*	*0*	*0*	*0*	*0*	*0*	*0*	*0*	*0*	*0*	*0*	*0*	*0*	*0*	*0*	*0*	*0*	*0*	*0*	*0.00*	*1*
0	0	0	0	0	0	0	0	0	0	−15	−15	−15	0	0	0	0	0	0	0	0	0.62	2
0	0	0	0	0	0	−10	0	0	0	−15	−15	0	−15	−15	0	0	0	0	0	0	0.93	3
0	0	0	0	0	0	0	0	0	0	−15	−15	0	0	0	0	0	0	0	0	0	0.51	4
0	0	0	0	0	0	0	0	0	0	30	−15	0	0	0	0	0	0	0	0	0	0.53	5
0	0	0	0	0	0	−10	0	0	0	15	−15	0	−15	−15	0	0	0	0	0	0	0.92	6
0	0	0	0	0	0	0	0	0	0	15	−15	0	0	0	0	0	0	0	0	0	0.51	7
0	0	0	0	0	0	−10	0	0	0	0	0	0	−15	−15	0	0	0	0	0	0	0.80	8
0	0	0	0	0	0	0	0	0	0	0	−15	0	0	0	0	0	0	0	0	0	0.51	9
0	0	0	0	0	0	0	0	0	0	15	0	0	0	0	0	0	−15	0	0	0	0.33	10
0	0	0	0	0	0	−10	0	0	0	−15	0	0	−15	−15	0	0	0	0	0	0	0.81	11
0	0	0	0	0	0	0	0	0	0	−15	15	−15	0	0	0	0	0	0	0	0	0.55	12
0	0	0	0	0	0	−10	0	0	0	0	−15	0	−15	−15	0	0	0	0	0	0	0.93	13
0	0	0	0	0	0	0	0	0	0	0	−15	−15	0	0	0	0	0	0	0	0	0.61	14
0	0	0	0	0	0	0	0	0	0	−15	0	0	0	0	0	0	0	0	0	0	0.00	15
0	0	0	0	0	0	0	0	0	0	−15	−15	0	0	0	0	0	0	15	0	0	0.57	16
0	0	0	0	0	0	0	0	0	0	−30	−15	0	0	0	0	0	0	0	0	0	0.53	17
0	0	0	0	0	0	−10	0	0	0	−30	−15	0	−15	−15	0	0	0	0	0	0	0.94	18
−10	0	0	0	0	0	−10	0	0	0	−15	−15	0	−15	0	0	0	0	0	0	0	1.27	19
0	0	0	0	0	0	0	0	0	0	30	0	0	0	0	0	0	0	0	0	0	0.00	20
0	0	0	0	0	0	0	0	0	0	15	−15	−15	0	0	0	0	0	0	0	0	0.62	21
0	0	0	0	0	0	0	0	0	0	0	0	0	0	0	0	0	−15	0	0	0	0.32	22
0	0	0	0	0	0	0	0	0	0	30	−15	0	0	0	0	0	0	15	0	0	0.58	23
−10	0	0	0	0	0	−10	0	0	0	−15	−15	0	−15	15	0	0	0	0	0	0	1.28	24

DOI: 10.1021/ci500523z
J. Chem. Inf. Model. 2015, 55, 614−627

Table 2. Comparison of H-Bonding Networks in TMs 1−2−7, TMs 2−3−4, and TMs 3−5−6 Regions for Each of the Predicted Conformations[a,b]

	TM1−TM2−TM7				TM2−TM3−TM4				TM3−TM5−TM6		
WT n-I/A[c]	N1.50-S7.46.46	D2.50-S7.46	D2.50-N7.49	T2.56-Y7.43	Y3.34-W4.50	K4.41-D3.49	K4.41-Y2.42	Y2.42-D3.49	R3.50-T6.34	R3.50-L6.30	R5.64-Y3.41
1-I	2.83	2.76	2.86	2.66	3.18	3.09	2.73	—	3.05	2.78	2.55
2-I	2.83	2.76	2.87	2.65	3.11	2.89	2.72	2.82	2.92	—	—
3-I	2.84	—	—	2.90	3.11	3.04	—	3.04	3.09	2.76	2.81
4-A	2.83	2.76	2.86	2.66	3.11	—	2.70	—	—	—	2.69
5-I	2.83	2.76	2.86	2.65	3.14	3.09	2.89	—	3.06	2.78	2.82
6-A	2.84	—	—	2.89	3.19	—	2.77	—	—	—	2.69
7-A	2.83	2.76	2.86	2.65	3.19	—	2.77	—	—	—	2.69
8-I	2.84	—	—	2.87	3.18	2.82	2.78	2.80	3.06	2.77	—
9-I	2.83	2.76	2.85	2.66	3.17	2.81	2.78	2.80	3.06	2.79	2.82
10-I	2.85	—	—	2.87	2.72	2.89	2.71	2.82	3.06	2.77	—
11-I	2.83	2.76	2.86	2.65	2.73	2.65	2.96	2.73	3.05	2.77	3.18
12-I	2.83	2.78	2.86	2.66	3.10	2.88	2.73	2.81	2.84	—	—
13-I	2.84	—	—	2.90	3.18	2.82	2.78	2.81	3.08	2.76	2.81
14-I	2.83	2.76	2.86	2.66	3.17	3.08	2.73	3.01	2.92	—	2.70
15-A	2.83	2.76	2.86	2.65	3.11	—	2.94	—	—	—	—
16-I	2.83	2.77	—	2.66	3.11	2.88	2.72	2.81	2.65	2.79	2.60
17-A	2.83	2.76	2.86	2.66	2.97	—	2.85	—	—	—	2.68
18-A	2.85	—	—	2.90	2.98	—	2.84	—	—	—	2.69
19-I	2.92	2.74	—	2.89	3.11	2.87	2.72	2.82	3.09	2.76	2.81
20-I	2.83	2.76	2.86	2.65	3.14	2.70	—	—	3.05	—	—
21-I	2.83	2.76	2.85	2.66	3.19	3.10	2.77	—	2.92	—	2.70
22-I	2.83	2.76	2.86	2.65	2.72	2.74	—	2.80	3.05	2.77	3.18
23-I	2.84	2.78	2.86	2.66	3.13	3.09	2.88	—	3.06	2.77	2.59
24-I	3.51	2.74	—	2.66	3.11	2.88	2.72	2.82	3.09	2.76	2.81

[a]Distances (Å) between heavy atoms of residues are present. [b]Also see Supporting Information Table S3. [c]WT n-I refer to the conformations that are supposed to be inactive, while WT n-A are supposed to be active.

DOI: 10.1021/ci500523z
J. Chem. Inf. Model. 2015, 55, 614−627

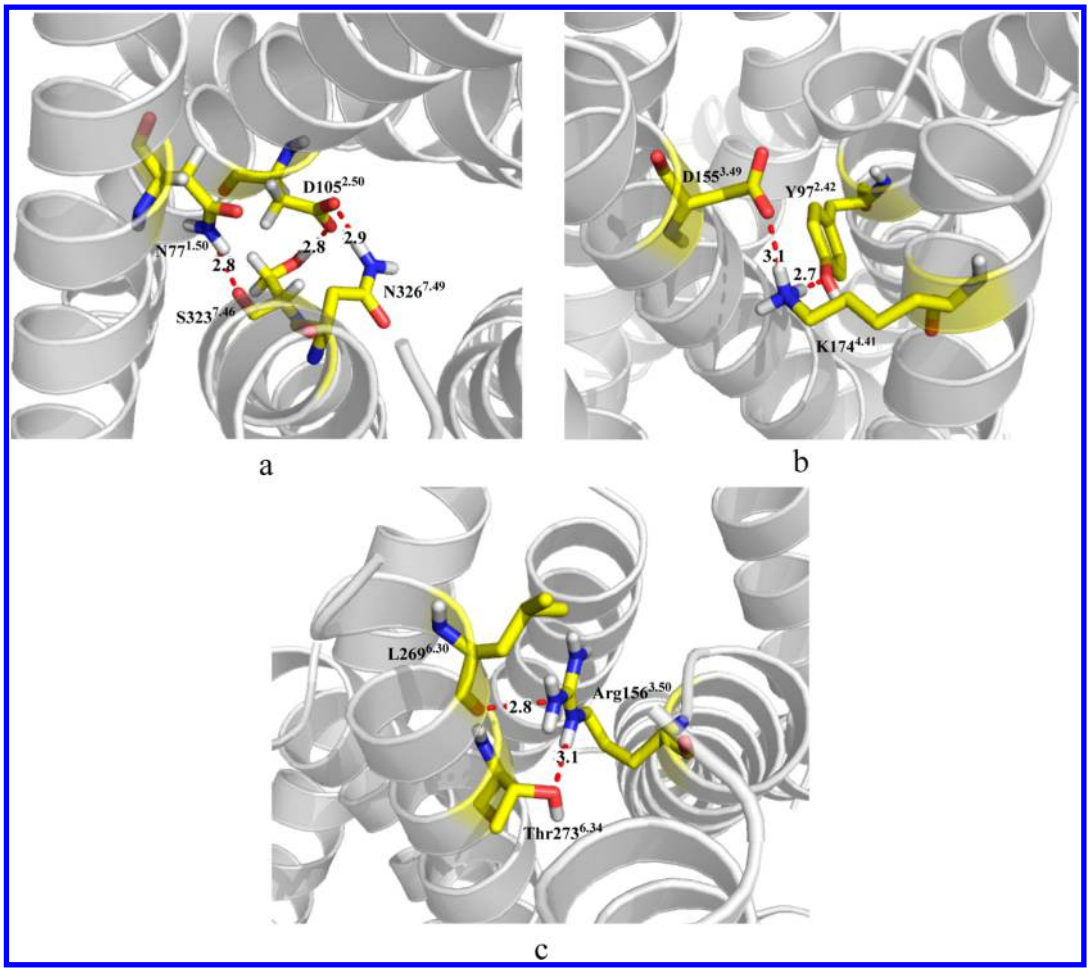

Figure 1. Hydrogen bond networks that enhance the stability of the TMs 1−2−7, TMs 2−3−4, and TMs 3−5−6 regions: (a) $N77^{1.50}$−$D105^{2.50}$−$S323^{7.46}$ hydrogen bond network. (b) $Y97^{2.42}$−$D155^{3.49}$−$K174^{4.41}$ hydrogen bond network. (c) TM3−TM6 ionic lock. The structures shown are for WT1.

optimization. At this point the protein side chains were dealanized using SCREAM to find the optimum side chains for each of the 100 poses. Then we neutralized the protein and the ligand by transferring protons appropriately within salt bridges and protonating or deprotonating exterior ligands, followed by further full geometry minimization. The final docked structure with the best binding energy was selected. Applying this procedure to the antagonist JDTic ligand in the X-ray structure led back to a structure deviating only 0.23 Å RMSD from the X-ray.

3.0. RESULTS AND DISCUSSION

3.1. Predictions of the Stable Structural Ensemble for κ-OR. The starting template for GEnSeMBLE predictions was the crystal structure of human κ-OR (PDB ID code 4DJH).[6] To find the optimum packings of the 7-helix bundle, we applied the BiHelix and ComBiHelix on the TM region.[21] This process sampled the η-angles from 0° to 360° in 30° increments to generate $(12)^7$ = 35 million combinations. The top 10 helix orientations are shown in Table S1, Supporting Information. We find that the all zero structure (X-ray structure) has the lowest energy, validating that the energy scoring and BiHelix procedure is reliable.

We then selected three of these structures (top1, top7, and top9) based on their structure and energy diversity and applied the SuperBiHelix and SuperComBiHelix methods.[14,15] Here we sampled η- and φ-angles from −30° to 30° in 15° increments and −10°, 0°, and 10° for the tilt angle, θ, leading to a total of $(5 \times 5 \times 3)^7$ = 13 trillion combinations, for each of which the energy was evaluated using the SuperBiHelix method. Finally we selected the best 24 structures in Table 1. Four different energies (charged total energy, charged interhelical energy, neutral total energy, and neutral interhelical energy) and their individual ranks associated with each of the TM bundle conformations sampled are shown in Supporting Information Table S2. The density of energy states throughout sampling are shown in Supporting Information Figure S1.

We found that the crystal structure (all zero structure, in italics) ranks first as the lowest energy conformation, which validates the energy scoring and SuperBiHelix procedures. There is no simple way to compare these structures, but the table compares the RMSD of the backbone to the human κ-OR crystal structure. Supporting Information Figure S2 shows the conformational diversity in predicted 24 low energy structures. The 23 other structures differ from the X-ray by 0.00 Å backbone RMSD (WT15 and WT20) to 1.28 Å (WT24). Thus, the members of the predicted ensemble of conformations are similar to the crystallographically characterized κ-OR. It is not known what is a reasonable RMSD difference between the conformations among active and inactive states, but we argue below that 6 of the 24 are probably active conformations.[29]

DOI: 10.1021/ci500523z
J. Chem. Inf. Model. 2015, 55, 614−627

Inspection of the three rotational angles shows that the sweep angles φ presents the most variation, especially in TM4 and TM5. In nearly all structures (except WT8 and WT22), TM4 and TM5 differ by 15° or 30° compared with the X-ray structure. These two helices are more flexible than others and may play a role in κ-OR activation. None of these structures shows any variation in TM2 and TM3. These two helices are nonflexible and locked in to preserve the conserved hydrogen bonding networks.

3.2. Analysis of Interhelix Interactions. For Class A GPCRs, several conserved interhelical interactions, such as the TMs 1−2−7 and TMs 2−3−4 hydrogen bond networks, are present in most crystal structures. These interactions are also found in all 24 for our predicted structures for κ-OR. To understand the differences between the different conformations in our ensemble, we analyzed the interhelical hydrogen bond interactions for each conformation (Table 2).

3.2.1. TM3−TM5−TM6 Interaction Network. A transmission switch in the TM3−TM5−TM6 helix interfaces has been observed in the agonist-induced activation process in GPCRs.[30−33] In particular the ionic lock formed between Arg$^{3.50}$ and Asp/Glu$^{6.30}$ is thought to stabilize the inactive conformation of rhodopsin and other rhodopsin-like Class A GPCRs,[34,35] so that conformations lacking this coupling might enhance constitutive activity.[36] Indeed in most X-ray structures for Class A GPCRs, there is a strong salt bridge between R3.50 (part of the DRY motif) and E/D6.30, both of which are conserved for many Class A GPCRs. This TM3−TM6 coupling has been observed in crystal structures of inactive GPCRs: bovine rhodopsin,[37] squid rhodopsin,[38,39] human dopamine D3 receptor,[34] thermally stabilized inactive turkey β1 adrenergic receptor,[36] and inactive human A_{2A} adenosine receptor mutants.[40] This ionic lock is thought to be critical in keeping the GPCR inactive, whereas its absence appears to be associated with GPCR activation. Indeed in GEnSeMBLE predictions on the CB1 receptor and confirmed by experiments, we showed that deliberately introducing mutations that break the 3−6 ionic lock leads to full constitutive activity while other mutations that introduce a 2−6 ionic lock in addition to the 3−6 lock lead to completely inactive configurations.[13]

However, human κ-OR has L269 at position 6.30 instead of Asp or Glu. Even so in the crystal structure (pictured in Figure 1c) the side chain of Thr273$^{6.34}$ forms a hydrogen bond lock with Arg156$^{3.50}$ and the backbone CO atom of L269$^{6.30}$ forms a hydrogen bond with Arg156$^{3.50}$. These interactions appear to stabilize the TM3 and TM6 coupling, which may keep κ-OR inactive so that breaking this interaction may lead to κ-OR activation.[6]

Of course for designing agonists more relevant is the structure for the active conformation. But little is known from experiment about the ensemble of conformations for κ-OR or the mechanism for conformational transitions. It has been possible to obtain X-ray structures for what must be active structures for other GPCRs by binding the G-Protein or the G_α fragment to the GPCR. However, this does not provide a detailed mapping of the conformational transition pathway.[41] Since GPCR activation occurs on the millisecond time scale, it is difficult for experiments to capture the pathway. In several active state crystal structures—bovine opsin,[42,43] bovine metrhodopsin II,[44] constitutively active mutant of bovine rhodopsin,[32] human β_2 adrenergic receptor (actHβ_2AR),[30,31,45] and human A_{2A} adenosine receptor (actHA_{2A}AR)[46,47]—a transmission switch in the TM3−TM5−TM6 helix interface was observed that results in breakdown of TM3−TM6 coupling and formation of a TM5−TM6 coupling. However, there is no information about the active structures for κ-OR.

We find that 18 of our 24 predicted structures exhibit this strong 3−6 coupling indicative of an inactive structure; however, WT4, WT6, WT7, WT15, WT17, and WT18 structures did not show TM3−TM6 coupling. Thus, we consider these 6 conformations as candidates for active structures. Evidence in favor of this interpretation is that structure WT15 provides the strongest binding to agonists morphine and nalorphine (see Table 3). Because the TM3−TM6 ionic lock is present in the other 18 predicted structures, we consider that these complexes are not activated. Of course, binding agonists to these structures may eventually break the 3−6 interaction as part of activation. Decoupling TM6 from TM3 would allow TM6 to move away from TM3 to interact with TM5 or TM7, which it does in the active conformation of the G protein-bound β_2-adrenergic receptor structure.[31]

Table 3. Calculated Binding Energies (kcal/mol) of Agonists Bond to Diverse Protein Conformations[a,b]

agonists	protein conformation	experimental pK_i	predicted binding energy	
			UnifiedCav	SnapBE
bremazocine	WT1-I	10.5	−34.89	−50.18
EKC	WT9-I	10.0	−32.89	−50.02
nalorphine	WT15-A	9.1	−30.70	−49.52
pentazocine	WT20-I	8.6	−27.26	−47.71
morphine	WT15-A	7.3	−32.45	−45.60

[a]UnifiedCav: unified cavity E is the nonbond energy between the ligand and the union of all protein residues within a constant cutoff distance of the ligand in all the complexes. SnapBE: vertical binding energy, snap binding E = complex E − protein E − ligand E. The binding studies were conducted on human opioid receptor-containing CHO cells.[71] These affinities are listed as pK_i values. [b]This data is plotted in Figure 6.

3.2.2. TM1−TM2−TM7 Interaction Network. A common feature of Class A GPCRs is the presence of a conserved hydrogen bonding network TM1.50 (N)−TM2.50 (D)−TM7.49 (N). The X-ray structure for κ-OR is slightly different, leading to

- D105$^{2.50}$−S323$^{7.46}$ with an HB distance of 2.76 Å. We find this in 18 out of 24 of our predicted structures (except for WT3, 6, 8, 10, 13, 18).
- D105$^{2.50}$−N326$^{7.49}$ with an HB distance of 2.86 Å. We find this in 15 out of 24 of our predicted structures (except for WT3, 6, 8, 10, 13, 16, 18, 19, 24). The lack of this HB differs from most Class A GPCRs. Instead there is a different 2−7 coupling.
- T111$^{2.56}$−Y320$^{7.43}$ with an HB distance of 2.66 Å. We find this in all of our predicted structures.
- N77$^{1.50}$−N326$^{7.49}$ do not interact. They have a closest interaction between heavy atoms of 5.52 Å. This distance is more than 5.50 Å in all 24 predicted structures. Instead there is a different 1−7 coupling.
- N77$^{1.50}$−S323$^{7.46}$ with an HB distance of 2.83 Å. We find this in all 24 predicted structures. This is an unusual coupling for Class A GPCRs, since this S323$^{7.46}$ is not conserved.

DOI: 10.1021/ci500523z
J. Chem. Inf. Model. 2015, 55, 614−627

We expected that the charged D2.50, highly conserved among most Class A GPCRs, would be associated with a positively charge entity, either H_3O^+ (or Na^+),[48] to achieve charge neutrality since it is buried, far away from the solvent. Indeed in many X-ray structures such a feature is observed.[31,46,49] This H_3O^+ would help stabilize the 1−2−7 coupling. A flaw with our current GEnSeMBLE method is that we do not include this charged H_3O^+ at any point in the 7-helix bundle calculations. As a result our predictions may lead to too many low lying structures that miss part of the 1−2−7 coupling. On the other hand, the X-ray structure for κ-OR does not show either a water or a Na^+ associated with D2.50. In addition, D2.50 did not interact with any carbonyl oxygen of nearby residues in the crystal structure. Thus, the good correspondence with the X-ray structure for the 1−2−7 region indicates that this is reasonable for κ-OR. For other GPCRs we often find that a water migrates to the D2.50 upon doing the molecular dynamic simulation on the full protein−membrane−water system.[50,51]

In any case it seems that κ-OR has strong 1−2−7 coupling even though it differs somewhat from that in other Class A GPCRs. We assume that this tight coupling of TMs 1, 2, and 7 is important to keep the TM1−TM2−TM7 region rigid for better control of activation.

3.2.3. TM2−TM3−TM4 Interaction Network. Class A GPCRs often have conserved couplings involving 2−3−4. Indeed the X-ray structure of κ-OR has three strong couplings, two involving Y97$^{2.42}$−D155$^{3.49}$−K174$^{4.41}$.

- K174$^{4.41}$−Y97$^{2.42}$ with an HB distance of 2.73 Å. This is not the normal interaction of Class A. We find this in 21 out of 24 for our predicted structures (except for WT3, 20, 22).
- K174$^{4.41}$−D155$^{3.49}$ with a salt bridge distance of 3.09 Å. D3.49 is the highly conserved residue of the D (E) RY motif in Class A GPCRs. This salt bridge has also been identified in the cannabinoid receptor one (CB1)[52] and is similar to the salt bridge between D3.49 and R4.37 in the crystal structure of the human CXCR4 chemokine receptor (hCXCR4).[13] We find this in 18 out of 24 of our predicted structures (except for WT4, 6, 7, 15, 17, 18).
- Y140$^{3.34}$−W183$^{4.50}$ with an HB distance of 3.18 Å. W4.50 is the highly conserved Trp in TM4, but this interaction is not the normal interaction of Class A. We find this in all 24 of our predicted structures.

This interaction network greatly stabilizes the TMs 2−3−4 region, particularly the ionic lock D155$^{3.49}$−K174$^{4.41}$, which is similar to the salt bridge between D3.49 and R4.37 in the hCXCR4 crystal[53] that was suggested to keep the GPCR inactive.[13]

In addition, we find many other hydrogen bond interactions that enhance the stability of the TMs 2−3−4 region. For example, the conserved residue W183$^{4.50}$ forms a strong hydrogen bond with the nonconserved residue Y140$^{3.34}$ in all 24 of our predicted structures. This interaction may be analogous to the conserved hydrogen bond interaction T148$^{3.42}$−W183$^{4.50}$ of other Class A GPCRs. In addition, other common hydrogen bond interactions involving 2−3−4 are N179$^{4.46}$−I96$^{2.41}$, K132$^{3.26}$−I194$^{4.61}$, K132$^{3.26}$−V195$^{4.62}$, and S186$^{4.53}$−T144$^{3.38}$, all of which were found in the X-ray structure and in most of our predicted conformations (listed in Supporting Information Table S3). Most of them were formed between TM3 and TM4.

The semiconserved TM2.45(S/N/T)−TM3.42(S/N/T)−TM4.50(W) hydrogen bond network observed in most Class A GPCRs was present in the crystal structure (WT1) and in 21 conformations (shown in Supporting Information Table S3). However, they locate closely to each other in all other structures, with the N100$^{2.45}$ + W183$^{4.50}$ distance ranging from 2.59 Å to 4.20 Å and the T148$^{3.42}$ + N100$^{2.45}$ distance ranging from 2.71 Å to 3.41 Å.

3.3. Comparison with GPCRs Whose Active and Inactive X-ray Structures Are Both Available. To further validate our models, we compared the predicted structures with three inactive−active pairs (rhodopsin[39,54−56]−opsin,[42,43] inactA_{2A}AR[40,57]−actA_{2A}AR,[46,47] and inactβ_2AR[12,58−60]−act-β_2AR[30,31,45]), whose active and inactive X-ray structures are both available. The structural transitions show common features for GPCR activation.

- In the rhodopsin−opsin activation model, the characteristic molecular switch is an ionic lock between R3.50 in TM3 and E6.30 in TM6. This ionic lock breaks during opsin activation;
- In the actA_{2A}AR, R3.50 and E6.30 are pulled farther apart to breakdown the ionic lock presented in fully inactHA_{2A}AR;
- Experimental studies also showed that protonation of E6.30 of the inactβ_2AR causes activation and that breaking of this ionic lock is necessary for full activation.

The C_α-C_α distance (between the C_α atoms of R3.50 and E6.30) and the N−O distance (the minimum distance between a guanidinium nitrogen atom of R3.50 and a carboxylate oxygen atom of E6.30) are listed in Supporting Information Table S4 for these GPCR crystal structures. The ionic locks were broken in all these active X-ray structures. Both the C_α−C_α distance and N−O distance are much larger than that in the inactive structures.

Because the human κ-OR lacks either of the acidic residues Asp/Glu at position 6.30, R3.50 forms a hydrogen bond to T6.34 in the inactive κ-OR structure. In all of our predicted top 24 structures for κ-OR, the C_α−C_α distance (∼6.1−7.1 Å) nearly does not change compared with the X-ray structure (7.1 Å). This is because large variations in TM3 and TM6 rotation are not observed in these low energy structures. However, we observe changes in the side chain rotamer of R3.50 in TM3 in 6 out of 24 structures (WT4, WT6, WT7, WT15, WT17, and WT18). The N−O distance becomes longer (∼3.9−4.9 Å) and the ionic lock breaks down. R3.50 is highly conserved in Class A GPCRs, and its rotameric state may have a role in GPCR activation. As has been discussed in section 3.2.1, these structures did not show any TM3−TM6 coupling and were supposed to be active. Because the TM3−TM6 ionic lock is present in the other 18 predicted structures, we consider that these complexes are not activated. The TM3−TM6 salt bridge is the most predominant feature to judge the activeness of GPCRs. In addition, we also compare the transmission switch in the seven TM helix interfaces.

- Opsin shows prominent structural changes in TM5−TM7, and TM6 is tilted outward by 6−7 Å compared to rhodopsin;
- actA_{2A}AR displays an outward tilt and rotation of TM6, a movement of TM5, and an axial shift of TM3;
- In actβ_2AR, a 11 Å outward movement of TM6 and rearrangements of TM5 and TM7 were observed.

It seems that the movements of TM5 and TM6 are common features in the activation of these three GPCRs. Our proposed six active κ-OR structures did not show variation of TM6. However, a large variation of TM5 and TM4 was observed instead. They sweep away from the center of the TM helix bundle by 15° or

DOI: 10.1021/ci500523z
J. Chem. Inf. Model. 2015, 55, 614−627

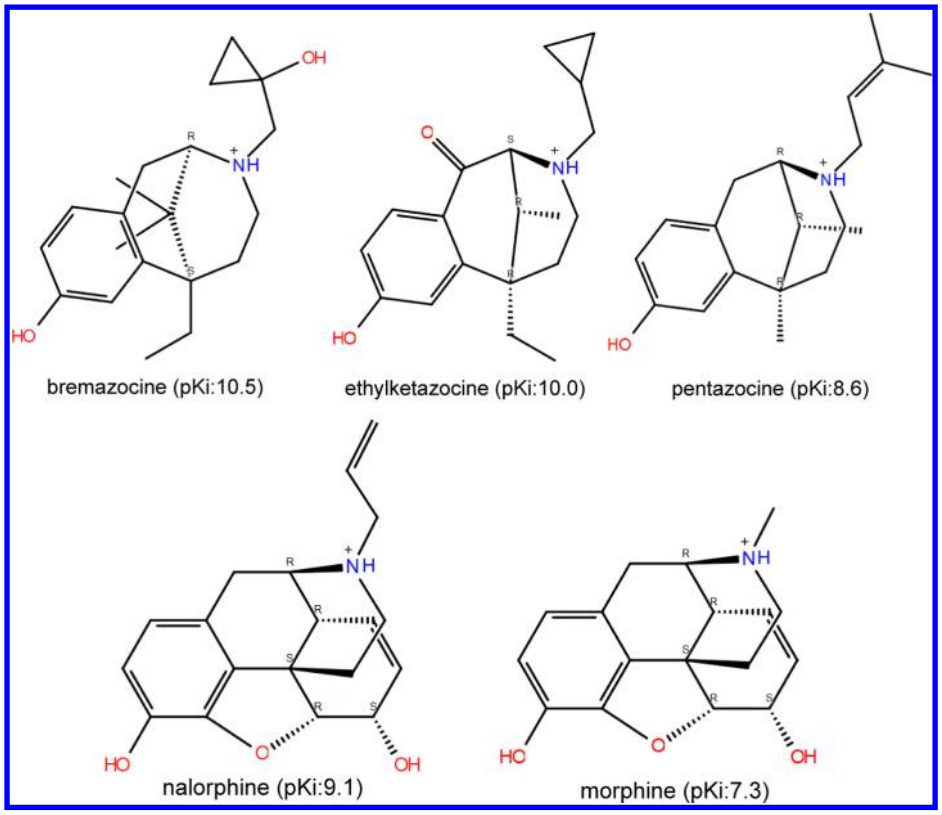

Figure 2. Chemical structures of structurally known κ-OR agonists in clinical study. The chiral centers of active enantiomers[72] for each agonist are labeled. The pK_i are from ref 71. On the basis of their pK_a values,[73,74] the tertiary N atoms of all these ligands are protonated at biological pH 7.4. Thus, the protonated form was used for docking.

30°, making more space available in the binding pocket. And also TM4 seems specific for κ-OR activation. The movement of TM4 leads to the breakdown of the K174$^{4.41}$−D155$^{3.49}$ salt bridge. As has been discussed in section 3.2.3, this salt bridge was suggested to keep the GPCR inactive. In company with the absence of TM3−TM6 ionic lock, the salt bridge K174$^{4.41}$−D155$^{3.49}$ also disappears in all six active κ-OR structures (Table 2). This further enhances the activeness of our predicted structures.

3.4. Ensemble Docking of Five Known κ-OR Selective Agonists to the Top 24 Predicted Conformations of κ-OR.

A number of κ-OR agonists have been used in clinical studies for the treatment of human disease.[61−63] Here we selected five, including three benzomorphans (ethylketocyclazocine,[64] bremazocine,[65] and pentazocine[66]) and two morphinans (nalorphine[67,68] and morphine[69]). Among these, pentazocine[66] and morphine[70] are approved drugs. Figure 2 shows the chemical structures and binding affinities (pK_i) of these agonists. Their structures are fairly rigid and have common pharmacophore components: the hydroxyl group, the benzene ring, and an amino group. In addition, all 5 binding constants are from the same set of experiments,[71] making comparison less problematic.

DarwinDock was used to dock all 5 compounds into the 24 predicted structures of κ-OR. This docking protocol was validated by redocking the crystal ligand JDTic to the crystal structure of the human κ-OR (PDB ID code 4DJH). JDTic was removed from the active site and docked back into the binding pocket. The nitrogen atoms in both the piperidine and isoquinoline moieties of JDTic were protonated. The RMSD between the predicted conformation and the observed X-ray crystallographic conformation of JDTic was 0.28 Å (Supporting Information Figure S3), validating that DarwinDock can predict accurate ligand−GPCR structures.

Each agonist was docked individually to all 24 predicted protein structures. The predicted ligand−protein structures for the three benzomorphans and two morphinans are shown in Figures 3 and 4, respectively. Figure 5 shows the superposition of these five binding sites. Our predicted snap binding energies are quite consistent with experimental constants (Table 3 and Figure 6). Figure 6 plots the calculated binding energies vs experimental pK_i. Note that ethylketocyclazocine, bremazocine, and pentazocine prefer protein structures expected to be inactive, while nalorphine and morphine prefer the same configuration WT15, expected to be active.

3.4.1. Predicted Binding Site of Ethylketocyclazocine (pK_i = 10.0). Ethylketocyclazocine [EKC] is a full agonist for κ-OR with a very high binding affinity (pK_i = 10.0).[71] We docked the active enantiomer[72] (−)-EKC to all the top 24 predicted protein structures. Most of the binding poses show salt bridges at D138$^{3.32}$ with the protonated nitrogen atom. The cavity analysis of the best binding site (Table 4) shows that the major contributing amino acids in ligand binding are D138$^{3.32}$ (−4.49 kcal/mol), H291$^{6.52}$ (−3.46 kcal/mol), W287$^{6.48}$ (−2.90 kcal/mol), Y139$^{3.33}$ (−2.39 kcal/mol), M142$^{3.36}$ (−2.07 kcal/mol), I290$^{6.51}$ (−1.60 kcal/mol), and V108$^{2.53}$ (−1.55 kcal/mol).

As is seen in Figure 3a, important elements of the binding sites are

- The protonated nitrogen atom forms a strong hydrogen bond with D138$^{3.32}$ in TM3. (Note that Figure 3a shows the neutralized structure used for energy calculations in which the proton is transferred to the D138$^{3.32}$). This is consistent with experiment since D138$^{3.32}$ is conserved in

DOI: 10.1021/ci500523z
J. Chem. Inf. Model. 2015, 55, 614−627

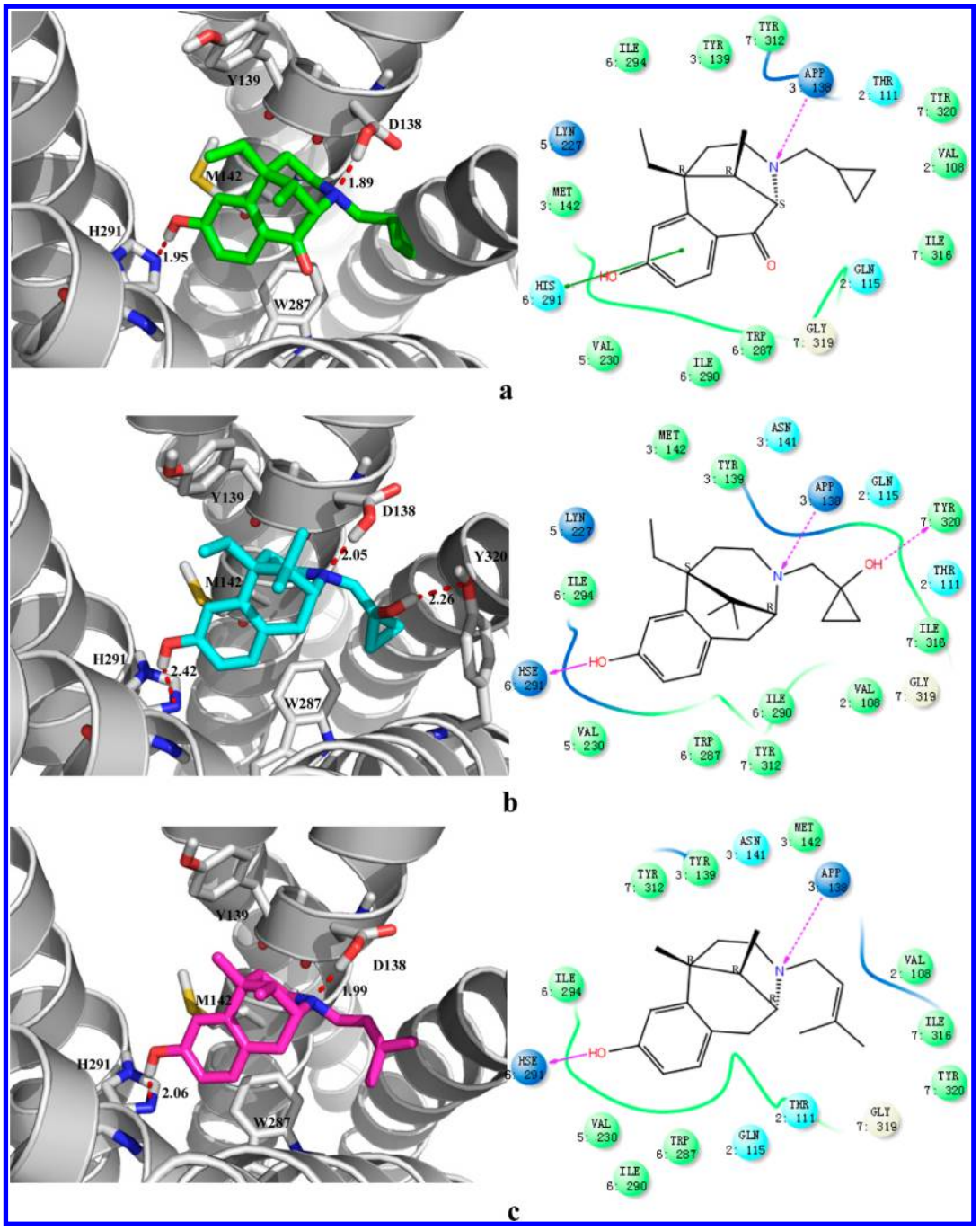

Figure 3. Predicted binding sites for the three benzomorphans bound to κ-OR: (a) ethylketocyclazocine, (b) bremazocine, and (c) pentazocine. Hydrogen bonds are represented by the arrows with the distance between the donor and the acceptor. Residues within 4 Å of each ligand are shown on the corresponding 2D ligand interaction diagram displayed at the right. For clarity, only polar hydrogen atoms are shown in the figure. Here the color code is that dark blue is charged, light blue is polar, green is hydrophobic, and white is glycine.

all opioid receptors and mutagenesis studies suggest that it plays an essential role in anchoring positively charged κ-OR ligands.[6,75,76]

- We find another hydrogen bond between the hydroxyl group of (−)-EKC and the imidazole ring of H291$^{6.52}$. This is consistent with experiment since the importance of this histidine in (−)-EKC binding has been underscored by site-directed mutagenesis experiments.[75,76] His291$^{6.52}$ has also been suggested to play a critical role in the receptor activation process.[6] The hydrogen bond linking the His291$^{6.52}$ imidazole ring to the phenolic hydroxyl group is typical for benzomorphans. This interaction was also found in previous docking studies.[77]
- In addition, we predict that the aromatic ring of (−)-EKC forms a strong hydrophobic contact with the conserved residue Trp287$^{6.48}$, which is thought to be a key part of the activation mechanism in many Class A GPCRs, including rhodopsin[32] and A_{2A}AR.[46] Similar hydrophobic contacts have been implicated in blocking activation-related conformational changes in the dark state of visual rhodopsin by 11-cis retinal and by inverse agonists in the A_{2A}AR and D3R.[6]

DOI: 10.1021/ci500523z
J. Chem. Inf. Model. 2015, 55, 614−627

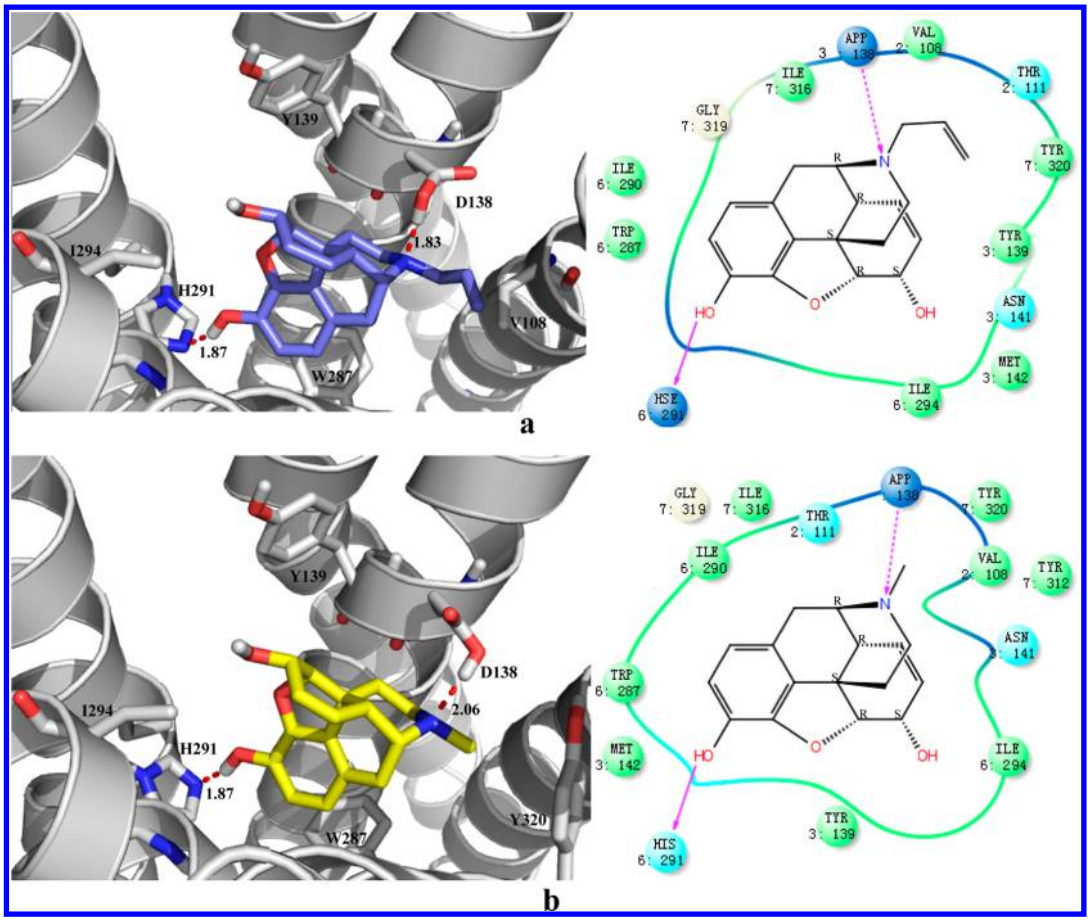

Figure 4. Predicted ligand−protein structures of the two morphinans: (a) nalorphine and (b) morphine. The H-bond is represented by the arrows with the distance between the donor and the acceptor. Residues within 4 Å of ligand are shown on the corresponding 2D ligand interaction diagram displayed on the right figure. For clarity, only polar hydrogen atoms were shown. Here the color code is that dark blue is charged, light blue is polar amino acid, green is nonpolar hydrophobic amino acid, and white is glycine.

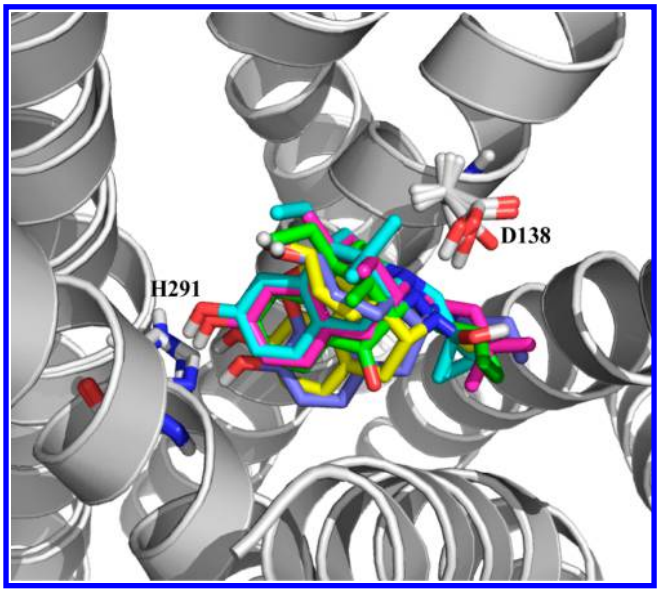

Figure 5. Superposition of all five binding sites. Color codes: EKC (green), bremazocine (cyan), pentazocine (magenta), nalorphine (purple), and morphine (yellow). For clarity, only polar hydrogen atoms were shown in the figure.

Since the crystal structure of the human κ-OR bound to the selective antagonist JDTic is available (PDB ID code 4DJH), we also compare the predicted EKC binding pose to the X-ray structure (Supporting Information Figure S4). The EKC binding pocket displays a combination of key characteristics both shared with and distinct from JDTic. Both of them are anchored by salt bridge interactions with D138$^{3.32}$ and form strong hydrophobic contact with the conserved residue Trp287$^{6.48}$. In contrast, the hydroxyl group of EKC dictates a little lower position of JDTic that is close to TM6. It forms a direct hydrogen bond with His291$^{6.52}$, which is thought to play a critical role in the receptor activation process.[6] In the crystal structure, several structured water molecules mediate polar interactions between the hydroxyl group and the receptor, but we do not consider waters in our DarwinDock predictions. The direct hydrogen bond interaction between EKC and His291$^{6.52}$ is consistent with EKC functioning as a κ-OR agonist.

Overall, the binding pose of (−)-EKC is in good agreement with the current generally accepted models.[78]

3.4.2. Rationalization of the Structure−Activity Relationships Based on Ethylketocyclazocine. The binding experiments found that small structural changes in the ligand lead to large changes in binding affinity. To validate the predicted binding site of (−)-EKC, we also docked the partial agonists bremazocine, pentazocine, nalorphine, and morphine. Due to their common structural skeleton, it is reasonable to assume that the binding sites of these additional four agonists to κ-OR would be similar to (−)-EKC. Indeed, Figure 5 shows the binding sites of these five agonists overlap, as expected. All show hydrogen bonds with

DOI: 10.1021/ci500523z
J. Chem. Inf. Model. 2015, 55, 614−627

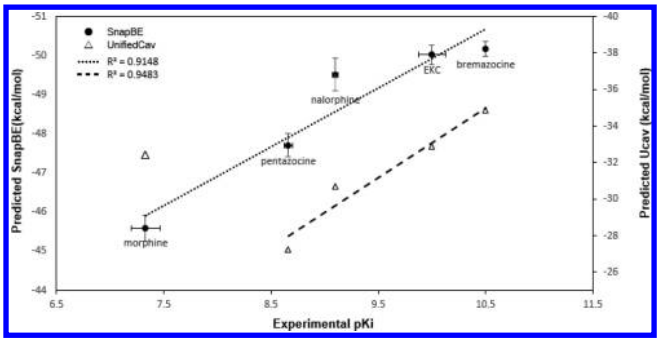

Figure 6. Comparison of the measured binding constants (pK_i) with experimental errors to the calculated binding energies (SnapBE)) for agonists listed in Table 3. For each ligand, we docked ~50 000 poses to the receptor's full conformational ensemble, from which we eventually select the best pose solely on the basis of energy. Bremazocine, EKC, nalorphine, pentazocine, and morphine bound to WT1-I, WT9-I, WT15-A, WT20-I, and WT15-A respectively. The SnapBE gives a good correlation with experiment (R^2 = 0.9148). SnapBE was used as scoring energy for the whole DarwinDock process because we consider it as most consistent for broad comparisons. However, we also show the UnifiedCav scoring energy. The correlation is good for all but morphine, which is predicted to bind too strongly by 2 kcal/mol. A major structural difference between morphine and the other four agonists is the substituent group on N. As is seen in Figure 2, this group is cyclopropylmethyl for EKC, (hydroxy-cyclopropyl)methyl for bremazocine, isoamylene for pentazocine, and allyl for nalorphine. But for morphine, it is just methyl. Due to its smaller size, morphine has more options and is more flexible when selecting a binding region. The experimental error is also large for morphine. Error bars for docking scores are shown as ±SEM with n = 10 for each data point.

Asp138$^{3.32}$ and His291$^{6.52}$. In addition all have an aromatic core that further enhances affinity with the hydrophilic/lipophilic groups of the ligand interacting with the hydrophobic cavity in the TMs 3−5−6 region (involving residues W287$^{6.48}$, I290$^{6.51}$, H291$^{6.52}$, V230$^{5.42}$, and M142$^{3.36}$). The constrained aliphatic 6-membered ring is surrounded by another hydrophobic cavity in TMs 2−3−7, with the protonated nitrogen interacting with the negative carboxylate of Asp138$^{3.32}$.

3.4.2a. Comparison of (−)-EKC to Bremazocine. As is shown in Figure 3b, bremazocine presents a binding pose similar to EKC. The protonated nitrogen atom interacts with the highly conserved residue Asp138$^{3.32}$. The hydroxyl group on the benzene ring forms strong hydrogen bond with His291$^{6.52}$. Compared with (−)-EKC, the introduction of another hydroxyl group substituted on the cyclopropane improves the binding affinity. This hydroxyl group forms a hydrogen bond with Try320$^{7.43}$ on TM7. The nonbond energy contributed by Try320$^{7.43}$ is −2.93 kcal/mol in bremazocine binding cavity, while it is −1.48 kcal/mol in EKC. A major structural difference between bremazocine and EKC is the ketonic oxygen site on EKC. From the cavity analysis for EKC this group seems too weak to provide a strong interaction with the receptor. The presence of this keto group was used to reduce stereoselectively and is beneficial for the bioisosteric replacement strategy.[72,74] The full unified cavity analysis of the hOPRK/bremazocine binding site is shown in Supporting Information Table S5.

3.4.2b. Comparison of (−)-EKC to (−)-Pentazocine. As is shown in Figure 3c, pentazocine also has the same binding pose as EKC. Compared with EKC, pentazocine has an unfavorable interaction at I290$^{6.51}$ (+6.26 kcal/mol) because of the bad contact with the isoamylene substitute group. This results in a dramatic decrease in binding affinity for pentazocine. This suggests that the steric effect of the N-substituent group should be considered when designing novel agonists for κ-OR. The full unified cavity analysis of the hOPRK/pentazocine binding site was shown in Supporting Information Table S6.

Table 4. Unified Cavity Energy of (−)-EKC Bound to Human Kappa Opioid Receptor[a]

residue	VdW	Coulomb	H-Bond	NonBond
APP 138	3.29	−3.70	−4.08	−4.49
HIS 291	2.39	−1.93	−3.92	−3.46
TRP 287	−2.96	0.06	0.00	−2.90
TYR 139	−2.31	−0.09	0.00	−2.39
MET 142	−2.30	0.23	0.00	−2.07
ILE 290	−1.42	−0.19	0.00	−1.60
VAL 108	−1.58	0.02	0.00	−1.55
GLN 115	−1.38	−0.11	0.00	−1.49
TYR 320	−1.33	−0.14	0.00	−1.48
ILE 294	−1.44	−0.03	0.00	−1.47
GLY 319	−0.78	−0.44	0.00	−1.22
TYR 312	−1.31	0.12	0.00	−1.19
ILE 316	−1.09	0.00	0.00	−1.08
VAL 230	−0.93	−0.06	0.00	−0.99
CYS 315	−0.54	−0.02	0.00	−0.56
LYN 227	−0.57	0.01	0.00	−0.55
ASN 141	−0.49	0.07	0.00	−0.42
THR 111	−0.47	0.05	0.00	−0.42
LEU 135	−0.35	−0.06	0.00	−0.41
ILE 137	−0.27	−0.10	0.00	−0.37
MET 112	−0.28	0.03	0.00	−0.26
PHE 293	−0.15	−0.06	0.00	−0.22
PHE 143	−0.21	0.00	0.00	−0.21
PRO 289	−0.15	−0.06	0.00	−0.21
PHE 231	−0.17	−0.03	0.00	−0.21

[a]The nonbonding (NonBond) energy is the sum of the components: van der Waals (vdW), Coulomb, and H-bond. We consider that the residues with contributions >1.00 are significant and that those above 3.00 are quite important. The cavity analysis for the other 4 ligands are in Supporting Information Tables S5, S6, S7, and S8. The residues are ordered by total NonBond energy, which is the sum of vdW, Coulomb, and H-bond energy (kcal/mol) in the unified cavity. Residues with contributions >0.20 are shown.

3.4.2c. Comparison of (−)-EKC to (−)-Nalorphine. Nalorphine also shows the same binding pose as EKC. As is seen in Figure 2, EKC lacks the cyclohexene ring of nalorphine and morphine. This structural modification for EKC was used to maximize the κ-OR selectivity and to minimize morphine-like side effects.[65,74,79−81] Although lacking a hydrophobic ring, the ethyl group of EKC contributes additional hydrophobic interactions with the receptor. Considering the two residues, Y139$^{3.33}$ and M142$^{3.36}$ near the ethyl, we see that Y139$^{3.33}$ contributes −2.39 kcal/mol in EKC but −1.66 kcal/mol in nalorphine, while M142$^{3.36}$ contributes −2.07 kcal/mol in EKC and −0.48 kcal/mol in nalorphine (Table 4 and Supporting Information Table S7). This may be why EKC has a higher binding affinity than nalorphine.

3.4.2d. Comparison of (−)-Nalorphine to Morphine. The only structural difference between nalorphine and morphine is the group on the N. It is an isopropyl in nalorphine and methyl in morphine. The allyl group contributes additional hydrophobic interaction to improve the binding affinity. So the N-substituted motif leads to increased affinity. Overall, the cavity analysis is quite similar.

DOI: 10.1021/ci500523z
J. Chem. Inf. Model. 2015, 55, 614−627

4.0. SUMMARY AND CONCLUSIONS

We predicted the ensemble of 24 low energy conformations for κ-OR using the GEnSeMBLE method which is extracted from a very complete set (~13 trillion configurations) of helix rotations and tilts.[21,22] The predicted lowest energy structure is the X-ray structure, validating the energy scoring and SuperBiHelix procedure. The analysis of the interhelical hydrogen bond networks finds salt bridges R3.50 + D6.34 and D3.49 + K4.41 are present in conformations that we expect to be inactive, since we assume that the TM3−TM6 couplings must break during activation in order for TM6 to bind to the G-Protein. Of the 24 conformations best for κ-OR, we find that six including WT15 may be active since they do not have the 3−6 coupling.

To further validate these structures, we used the DarwinDock method to predict the binding sites for five known agonists bound to κ-OR. We find that bremazocine binds preferentially to protein configuration WT1 corresponding to the X-ray structure, while EKC and pentazocine also prefer inactive conformations (WT9 and WT20, respectively). However, both nalorphine and morphine prefer the active configuration WT15. This information should be useful in designing ligands with selectivity for a particular signaling pathway, "functional selectivity". We find that superposition of these selective agonists indicates a common pharmacophore with similar arrangements at the same binding site:

- The protonated nitrogen forms a salt bridge with conserved D138$^{3.21}$;
- The hydroxyl group shows direct hydrogen binding with H291$^{6.52}$;
- The aromatic ring substituted with the hydroxyl groups interacts with lipophilic pockets in TMs 3−5−6, which involves residues W287$^{6.48}$, I290$^{6.51}$, H291$^{6.52}$, V230$^{5.42}$, and M142$^{3.36}$;
- And the aliphatic ring is located in TMs 2−3−7 and is surrounded by residues V108$^{2.53}$, Y139$^{3.33}$, I316$^{7.39}$, Y320$^{7.43}$, G319$^{7.42}$, and Y312$^{7.35}$.

These 3D ligand−protein structures and apoprotein structures for κ-OR should be useful for guiding drug design, providing a structural basis for exploring how ligand binding is related to receptor activation of κ-OR (and other Class A GPCRs). Since EKC and bremazocine are the two most strongly bound agonists of the five we considered, one may use the predicted ligand−protein structure to suggest changes in the ligand that might improve binding. Thus, we suggest introducing hydrophobic centers, such as the cyclopropane and allyl group, on the tertiary N atom and also hydrogen bond acceptor/donors, such as the hydroxyl group, on this N-substitute group.

■ ASSOCIATED CONTENT

Supporting Information

Details of GEnSeMBLE prediction of the 3D structure of human kappa opioid receptor (κ-OR) (Text S1); coordinates of predicted structure (WT1) for κ-OR (Text S2); top 10 BiHelix structures for k-OR (η) (Table S1); four kinds of energies and their individual ranks for predicted 24 κ-OR structures (Table S2); hydrogen bond networks in TMs 2−3−4 and TMs 6−7 regions of top 24 conformations (Table S3); comparison of ionic lock conformations in GPCR crystal structures (Table S4); unified cavity energy of bremazocine, pentazocine, nalorphine, and morphine bound to human kappa opioid receptor (Tables S5, S6, S7, and S8); density of states based on four kinds of energies throughout the 2000 best receptor bundles (Figure S1); side and extracellular view of the conformational diversity in predicted 24 low energy structures (Figure S2); comparison of JDTic pose in the crystal structure and that from DarwinDock (Figure S3); and positions of ligands in superimposed crystal structure of human k-OR and our predicted k-OR structure WT9 (Figure S4). This material is available free of charge via the Internet at http://pubs.acs.org.

■ AUTHOR INFORMATION

Corresponding Author

*E-mail: wag@wag.caltech.edu.

Notes

The authors declare no competing financial interest.

■ ACKNOWLEDGMENTS

We thank Prof. Ravinder Abrol and Mr. Adam Griffith for many helpful discussions. This work was supported by grants from China Scholarship Council and by gifts to the Materials and Process Simulation Center. The computational resources were provided the NSF-CSEM grant to Caltech and the DURIP-ONR grant to W.A.G.

■ REFERENCES

(1) Dhawan, B. N.; Cesselin, F.; Raghubir, R.; Reisine, T.; Bradley, P. B.; Portoghese, P. S.; Hamon, M. International Union of Pharmacology. XII. Classification of Opioid Receptors. *Pharmacol. Rev.* **1996**, *48*, 567−592.

(2) Waldhoer, M.; Bartlett, S. E.; Whistler, J. L. Opioid Receptors. *Annu. Rev. Biochem.* **2004**, *73*, 953−990.

(3) Thompson, A. A.; Liu, W.; Chun, E.; Katritch, V.; Wu, H.; Vardy, E.; Huang, X. P.; Trapella, C.; Guerrini, R.; Calo, G.; Roth, B. L.; Cherezov, V.; Stevens, R. C. Structure of the Nociceptin/Orphanin FQ Receptor in Complex with a Peptide Mimetic. *Nature* **2012**, *485*, 395−399.

(4) Granier, S.; Manglik, A.; Kruse, A. C.; Kobilka, T. S.; Thian, F. S.; Weis, W. I.; Kobilka, B. K. Structure of the Delta-Opioid Receptor Bound to Naltrindole. *Nature* **2012**, *485*, 400−404.

(5) Manglik, A.; Kruse, A. C.; Kobilka, T. S.; Thian, F. S.; Mathiesen, J. M.; Sunahara, R. K.; Pardo, L.; Weis, W. I.; Kobilka, B. K.; Granier, S. Crystal Structure of the Micro-Opioid Receptor Bound to a Morphinan Antagonist. *Nature* **2012**, *485*, 321−326.

(6) Wu, H.; Wacker, D.; Mileni, M.; Katritch, V.; Han, G. W.; Vardy, E.; Liu, W.; Thompson, A. A.; Huang, X. P.; Carroll, F. I.; Mascarella, S. W.; Westkaemper, R. B.; Mosier, P. D.; Roth, B. L.; Cherezov, V.; Stevens, R. C. Structure of the Human Kappa-Opioid Receptor in Complex with JDTic. *Nature* **2012**, *485*, 327−332.

(7) Martin, W. R.; Eades, C. G.; Thompson, J. A.; Huppler, R. E.; Gilbert, P. E. The Effects of Morphine- and Nalorphine- Like Drugs in the Nondependent and Morphine-Dependent Chronic Spinal Dog. *J. Pharmacol. Exp. Ther.* **1976**, *197*, 517−532.

(8) Simonin, F.; Gaveriaux-Ruff, C.; Befort, K.; Matthes, H.; Lannes, B.; Micheletti, G.; Mattei, M. G.; Charron, G.; Bloch, B.; Kieffer, B. Kappa-Opioid Receptor in Humans: cDNA and Genomic Cloning, Chromosomal Assignment, Functional Expression, Pharmacology, and Expression Pattern in the Central Nervous System. *Proc. Natl. Acad. Sci. U. S. A.* **1995**, *92*, 7006−7010.

(9) Carlezon, W. A., Jr.; Beguin, C.; Knoll, A. T.; Cohen, B. M. Kappa-Opioid Ligands in the Study and Treatment of Mood Disorders. *Pharmacol. Ther.* **2009**, *123*, 334−343.

(10) Urban, J. D.; Clarke, W. P.; von Zastrow, M.; Nichols, D. E.; Kobilka, B.; Weinstein, H.; Javitch, J. A.; Roth, B. L.; Christopoulos, A.; Sexton, P. M.; Miller, K. J.; Spedding, M.; Mailman, R. B. Functional Selectivity and Classical Concepts of Quantitative Pharmacology. *J. Pharmacol. Exp. Ther.* **2007**, *320*, 1−13.

(11) Yao, X. J.; Velez Ruiz, G.; Whorton, M. R.; Rasmussen, S. G.; DeVree, B. T.; Deupi, X.; Sunahara, R. K.; Kobilka, B. The Effect of

DOI: 10.1021/ci500523z
J. Chem. Inf. Model. 2015, 55, 614−627

Ligand Efficacy on the Formation and Stability of a GPCR-G Protein Complex. *Proc. Natl. Acad. Sci. U. S. A.* **2009**, *106*, 9501−9506.
(12) Bhattacharya, S.; Hall, S. E.; Li, H.; Vaidehi, N. Ligand-Stabilized Conformational States of Human Beta(2) Adrenergic Receptor: Insight into G-Protein-Coupled Receptor Activation. *Biophys. J.* **2008**, *94*, 2027−2042.
(13) Scott, C. E.; Abrol, R.; Ahn, K. H.; Kendall, D. A.; Goddard, W. A., III. Molecular Basis for Dramatic Changes in Cannabinoid CB1 G protein-Coupled Receptor Activation Upon Single and Double Point Mutations. *Protein Sci.* **2013**, *22*, 101−113.
(14) Abrol, R.; Griffith, A. R.; Bray, J. K.; Goddard, W. A., III. Structure Prediction of G Protein-Coupled Receptors and their Ensemble of Functionally Important Conformations. *Methods Mol. Biol.* **2012**, *914*, 237−254.
(15) Abrol, R.; Kim, S. K.; Bray, J. K.; Trzaskowski, B.; Goddard, W. A., III. Conformational Ensemble View of G Protein-Coupled Receptors and the Effect of Mutations and Ligand Binding. *Methods Enzymol.* **2013**, *520*, 31−48.
(16) Kim, S. K.; Riley, L.; Abrol, R.; Jacobson, K. A.; Goddard, W. A., III. Predicted Structures of Agonist and Antagonist Bound Complexes of Adenosine A3 Receptor. *Proteins* **2011**, *79*, 1878−1897.
(17) Charlier, L.; Topin, J.; Ronin, C.; Kim, S. K.; Goddard, W. A., III; Efremov, R.; Golebiowski, J. How Broadly Tuned Olfactory Receptors Equally Recognize their Agonists. Human OR1G1 as a Test Case. *Cell. Mol. Life Sci.* **2012**, *69*, 4205−4213.
(18) Berro, R.; Yasmeen, A.; Abrol, R.; Trzaskowski, B.; Abi-Habib, S.; Grunbeck, A.; Lascano, D.; Goddard, W. A., III; Klasse, P. J.; Sakmar, T. P.; Moore, J. P. Use of G-Protein-Coupled and -Uncoupled CCR5 Receptors by CCR5 Inhibitor-Resistant and -Sensitive Human Immunodeficiency Virus Type 1 Variants. *J. Virol.* **2013**, *87*, 6569−6581.
(19) Abrol, R.; Trzaskowski, B.; Goddard, W. A., III; Nesterov, A.; Olave, I. Ligand- and Mutation-Induced Conformational Selection in the CCR5 Chemokine G Protein-Coupled Receptor. *Proc. Natl. Acad. Sci. U. S. A.* **2014**, *111*, 13040−13045.
(20) Vaidehi, N.; Kenakin, T. The Role of Conformational Ensembles of Seven Transmembrane Receptors in Functional Selectivity. *Curr. Opin. Pharmacol.* **2010**, *10*, 775−781.
(21) Abrol, R.; Bray, J. K.; Goddard, W. A., III. Bihelix: Towards de Novo Structure Prediction of an Ensemble of G-Protein Coupled Receptor Conformations. *Proteins* **2011**, *80*, 505−518.
(22) Bray, J. K.; Abrol, R.; Goddard, W. A., III; Trzaskowski, B.; Scott, C. E. SuperBiHelix Method for Predicting the Pleiotropic Ensemble of G-Protein-Coupled Receptor Conformations. *Proc. Natl. Acad. Sci. U. S. A.* **2014**, *111*, E72−E78.
(23) Kirkpatrick, A.; Heo, J.; Abrol, R.; Goddard, W. A., III. Predicted Structure of Agonist-Bound Glucagon-Like Peptide 1 Receptor, a Class B G Protein-Coupled Receptor. *Proc. Natl. Acad. Sci. U. S. A.* **2012**, *109*, 19988−19993.
(24) Tan, J.; Abrol, R.; Trzaskowski, B.; Goddard, W. A., III. 3D Structure Prediction of TAS2R38 Bitter Receptors Bound to Agonists Phenylthiocarbamide (PTC) and 6-n-Propylthiouracil (PROP). *J. Chem. Inf. Model.* **2012**, *52*, 1875−1885.
(25) Mayo, S. L.; Olafson, B. D; Goddard, W. A., III. DREIDING: a Generic Force Field for Molecular Simulations. *J. Phys. Chem.* **1990**, *94*, 8897−8909.
(26) Wimley, W. C.; Creamer, T. P.; White, S. H. Solvation Energies of Amino Acid Side Chains and Backbone in a Family of Host-Guest Pentapeptides. *Biochemistry* **1996**, *35*, 5109−5124.
(27) Wai Tak Kam, V.; Goddard, W. A., III. Flat-Bottom Strategy for Improved Accuracy in Protein Side-Chain Placements. *J. Chem. Theory Comput.* **2008**, *4*, 2160−2169.
(28) Ewing, T. J.; Makino, S.; Skillman, A. G.; Kuntz, I. D. DOCK 4.0: Search Strategies for Automated Molecular Docking of Flexible Molecule Databases. *J. Comput.-Aided Mol. Des.* **2001**, *15*, 411−428.
(29) Boehr, D. D.; Nussinov, R.; Wright, P. E. The Role of Dynamic Conformational Ensembles in Biomolecular Recognition. *Nat. Chem. Biol.* **2009**, *5*, 789−796.
(30) Rasmussen, S. G.; Choi, H. J.; Fung, J. J.; Pardon, E.; Casarosa, P.; Chae, P. S.; Devree, B. T.; Rosenbaum, D. M.; Thian, F. S.; Kobilka, T. S.; Schnapp, A.; Konetzki, I.; Sunahara, R. K.; Gellman, S. H.; Pautsch, A.; Steyaert, J.; Weis, W. I.; Kobilka, B. K. Structure of a Nanobody-Stabilized Active State of the Beta(2) Adrenoceptor. *Nature* **2011**, *469*, 175−180.
(31) Rasmussen, S. G.; DeVree, B. T.; Zou, Y.; Kruse, A. C.; Chung, K. Y.; Kobilka, T. S.; Thian, F. S.; Chae, P. S.; Pardon, E.; Calinski, D.; Mathiesen, J. M.; Shah, S. T.; Lyons, J. A.; Caffrey, M.; Gellman, S. H.; Steyaert, J.; Skiniotis, G.; Weis, W. I.; Sunahara, R. K.; Kobilka, B. K. Crystal Structure of the Beta2 Adrenergic Receptor-Gs Protein Complex. *Nature* **2011**, *477*, 549−555.
(32) Standfuss, J.; Edwards, P. C.; D'Antona, A.; Fransen, M.; Xie, G.; Oprian, D. D.; Schertler, G. F. The Structural Basis of Agonist-Induced Activation in Constitutively Active Rhodopsin. *Nature* **2011**, *471*, 656−660.
(33) Deupi, X.; Standfuss, J. Structural Insights into Agonist-Induced Activation of G-Protein-Coupled Receptors. *Curr. Opin. Struct. Biol.* **2011**, *21*, 541−551.
(34) Chien, E. Y.; Liu, W.; Zhao, Q.; Katritch, V.; Han, G. W.; Hanson, M. A.; Shi, L.; Newman, A. H.; Javitch, J. A.; Cherezov, V.; Stevens, R. C. Structure of the Human Dopamine D3 Receptor in Complex with a D2/D3 Selective Antagonist. *Science* **2010**, *330*, 1091−1095.
(35) Palczewski, K.; Kumasaka, T.; Hori, T.; Behnke, C. A.; Motoshima, H.; Fox, B. A.; Le Trong, I.; Teller, D. C.; Okada, T.; Stenkamp, R. E.; Yamamoto, M.; Miyano, M. Crystal Structure of Rhodopsin: a G Protein-Coupled Receptor. *Science* **2000**, *289*, 739−745.
(36) Warne, T.; Serrano-Vega, M. J.; Baker, J. G.; Moukhametzianov, R.; Edwards, P. C.; Henderson, R.; Leslie, A. G.; Tate, C. G.; Schertler, G. F. Structure of a Beta1-Adrenergic G-Protein-Coupled Receptor. *Nature* **2008**, *454*, 486−491.
(37) Bourne, H. R.; Meng, E. C. Structure. Rhodopsin Sees the Light. *Science* **2000**, *289*, 733−734.
(38) Murakami, M.; Kouyama, T. Crystal Structure of Squid Rhodopsin. *Nature* **2008**, *453*, 363−367.
(39) Shimamura, T.; Hiraki, K.; Takahashi, N.; Hori, T.; Ago, H.; Masuda, K.; Takio, K.; Ishiguro, M.; Miyano, M. Crystal Structure of Squid Rhodopsin with Intracellularly Extended Cytoplasmic Region. *J. Biol. Chem.* **2008**, *283*, 17753−17756.
(40) Dore, A. S.; Robertson, N.; Errey, J. C.; Ng, I.; Hollenstein, K.; Tehan, B.; Hurrell, E.; Bennett, K.; Congreve, M.; Magnani, F.; Tate, C. G.; Weir, M.; Marshall, F. H. Structure of the Adenosine A(2A) Receptor in Complex with ZM241385 and the Xanthines XAC and Caffeine. *Structure* **2011**, *19*, 1283−1293.
(41) Niesen, M. J.; Bhattacharya, S.; Vaidehi, N. The Role of Conformational Ensembles in Ligand Recognition in G-Protein Coupled Receptors. *J. Am. Chem. Soc.* **2011**, *133*, 13197−13204.
(42) Park, J. H.; Scheerer, P.; Hofmann, K. P.; Choe, H. W.; Ernst, O. P. Crystal Structure of the Ligand-Free G-Protein-Coupled Receptor Opsin. *Nature* **2008**, *454*, 183−187.
(43) Scheerer, P.; Park, J. H.; Hildebrand, P. W.; Kim, Y. J.; Krauss, N.; Choe, H. W.; Hofmann, K. P.; Ernst, O. P. Crystal Structure of Opsin in its G-Protein-Interacting Conformation. *Nature* **2008**, *455*, 497−502.
(44) Choe, H. W.; Kim, Y. J.; Park, J. H.; Morizumi, T.; Pai, E. F.; Krauss, N.; Hofmann, K. P.; Scheerer, P.; Ernst, O. P. Crystal Structure of Metarhodopsin II. *Nature* **2011**, *471*, 651−655.
(45) Rosenbaum, D. M.; Zhang, C.; Lyons, J. A.; Holl, R.; Aragao, D.; Arlow, D. H.; Rasmussen, S. G.; Choi, H. J.; Devree, B. T.; Sunahara, R. K.; Chae, P. S.; Gellman, S. H.; Dror, R. O.; Shaw, D. E.; Weis, W. I.; Caffrey, M.; Gmeiner, P.; Kobilka, B. K. Structure and Function of an Irreversible Agonist-Beta(2) Adrenoceptor Complex. *Nature* **2011**, *469*, 236−240.
(46) Xu, F.; Wu, H.; Katritch, V.; Han, G. W.; Jacobson, K. A.; Gao, Z. G.; Cherezov, V.; Stevens, R. C. Structure of an Agonist-Bound Human A2A Adenosine Receptor. *Science* **2011**, *332*, 322−327.
(47) Lebon, G.; Warne, T.; Edwards, P. C.; Bennett, K.; Langmead, C. J.; Leslie, A. G.; Tate, C. G. Agonist-Bound Adenosine A2A Receptor Structures Reveal Common Features of GPCR Activation. *Nature* **2011**, *474*, 521−525.

DOI: 10.1021/ci500523z
J. Chem. Inf. Model. 2015, 55, 614−627

(48) Katritch, V.; Fenalti, G.; Abola, E. E.; Roth, B. L.; Cherezov, V.; Stevens, R. C. Allosteric Sodium in Class A GPCR Signaling. *Trends Biochem. Sci.* **2014**, *39*, 233−244.
(49) Liu, W.; Chun, E.; Thompson, A. A.; Chubukov, P.; Xu, F.; Katritch, V.; Han, G. W.; Roth, C. B.; Heitman, L. H.; AP, I. J.; Cherezov, V.; Stevens, R. C. Structural Basis for Allosteric Regulation of GPCRs by Sodium Ions. *Science* **2012**, *337*, 232−236.
(50) Pardo, L.; Deupi, X.; Dolker, N.; Lopez-Rodriguez, M. L.; Campillo, M. The Role of Internal Water Molecules in the Structure and Function of the Rhodopsin Family of G Protein-Coupled Receptors. *ChemBioChem* **2007**, *8*, 19−24.
(51) Slusarz, M. J.; Slusarz, R.; Ciarkowski, J. Molecular Dynamics Study of the Internal Water Molecules in Vasopressin and Oxytocin Receptors. *Protein Pept. Lett.* **2009**, *16*, 342−350.
(52) Ahn, K. H.; Scott, C. E.; Abrol, R.; Goddard, W. A., III; Kendall, D. A. Computationally-Predicted CB1 Cannabinoid Receptor Mutants Show Distinct Patterns of Salt-Bridges that Correlate with their Level of Constitutive Activity Reflected in G Protein Coupling Levels, Thermal Stability, and Ligand Binding. *Proteins* **2013**, *81*, 1304−1317.
(53) Wu, B.; Chien, E. Y.; Mol, C. D.; Fenalti, G.; Liu, W.; Katritch, V.; Abagyan, R.; Brooun, A.; Wells, P.; Bi, F. C.; Hamel, D. J.; Kuhn, P.; Handel, T. M.; Cherezov, V.; Stevens, R. C. Structures of the CXCR4 Chemokine GPCR with Small-Molecule and Cyclic Peptide Antagonists. *Science* **2010**, *330*, 1066−1071.
(54) Okada, T.; Sugihara, M.; Bondar, A. N.; Elstner, M.; Entel, P.; Buss, V. The Retinal Conformation and its Environment in Rhodopsin in Light of a New 2.2 Å Crystal Structure. *J. Mol. Biol.* **2004**, *342*, 571−583.
(55) Okada, T.; Fujiyoshi, Y.; Silow, M.; Navarro, J.; Landau, E. M.; Shichida, Y. Functional Role of Internal Water Molecules in Rhodopsin Revealed by X-ray Crystallography. *Proc. Natl. Acad. Sci. U. S. A.* **2002**, *99*, 5982−5987.
(56) Li, J.; Edwards, P. C.; Burghammer, M.; Villa, C.; Schertler, G. F. Structure of Bovine Rhodopsin in a Trigonal Crystal Form. *J. Mol. Biol.* **2004**, *343*, 1409−1438.
(57) Jones, L. L.; Colf, L. A.; Bankovich, A. J.; Stone, J. D.; Gao, Y. G.; Chan, C. M.; Huang, R. H.; Garcia, K. C.; Kranz, D. M. Different Thermodynamic Binding Mechanisms and Peptide Fine Specificities Associated With a Panel of Structurally Similar High-Affinity T Cell Receptors. *Biochemistry* **2008**, *47*, 12398−12408.
(58) Cherezov, V.; Rosenbaum, D. M.; Hanson, M. A.; Rasmussen, S. G.; Thian, F. S.; Kobilka, T. S.; Choi, H. J.; Kuhn, P.; Weis, W. I.; Kobilka, B. K.; Stevens, R. C. High-Resolution Crystal Structure of an Engineered Human Beta2-Adrenergic G Protein-Coupled Receptor. *Science* **2007**, *318*, 1258−1265.
(59) Hanson, M. A.; Cherezov, V.; Griffith, M. T.; Roth, C. B.; Jaakola, V. P.; Chien, E. Y.; Velasquez, J.; Kuhn, P.; Stevens, R. C. A Specific Cholesterol Binding Site is Established by the 2.8 Å Structure of the Human Beta2-Adrenergic Receptor. *Structure* **2008**, *16*, 897−905.
(60) Rasmussen, S. G.; Choi, H. J.; Rosenbaum, D. M.; Kobilka, T. S.; Thian, F. S.; Edwards, P. C.; Burghammer, M.; Ratnala, V. R.; Sanishvili, R.; Fischetti, R. F.; Schertler, G. F.; Weis, W. I.; Kobilka, B. K. Crystal Structure of the Human Beta2 Adrenergic G-Protein-Coupled Receptor. *Nature* **2007**, *450*, 383−387.
(61) Pfeiffer, A.; Brantl, V.; Herz, A.; Emrich, H. M. Psychotomimesis Mediated by Kappa Opiate Receptors. *Science* **1986**, *233*, 774−776.
(62) Chavkin, C.; James, I. F.; Goldstein, A. Dynorphin is a Specific Endogenous Ligand of the Kappa Opioid Receptor. *Science* **1982**, *215*, 413−415.
(63) Williams, K.; Lee, E. Importance of Drug Enantiomers in Clinical Pharmacology. *Drugs* **1985**, *30*, 333−354.
(64) Pasternak, G. W. Multiple opiate receptors: [3H]-Ethylketocyclazocine Receptor Binding and Ketocyclazocine Analgesia. *Proc. Natl. Acad. Sci. U. S. A.* **1980**, *77*, 3691−3694.
(65) Dortch-Carnes, J.; Potter, D. E. Bremazocine: a Kappa-Opioid Agonist with Potent Analgesic and other Pharmacologic Properties. *CNS Drug Rev.* **2005**, *11*, 195−212.
(66) Brogden, R. N.; Speight, T. M.; Avery, G. S. Pentazocine: a Review of its Pharmacological Properties, Therapeutic Efficacy and Dependence Liability. *Drugs* **1973**, *5*, 6−91.
(67) Keats, A. S.; Telford, J. Nalorphine, a Potent Analgesic in Man. *J. Pharmacol. Exp. Ther.* **1956**, *117*, 190−196.
(68) Paul, D.; Pick, C. G.; Tive, L. A.; Pasternak, G. W. Pharmacological Characterization of Nalorphine, a Kappa 3 Analgesic. *J. Pharmacol. Exp. Ther.* **1991**, *257*, 1−7.
(69) Osborne, R.; Joel, S.; Trew, D.; Slevin, M. Morphine and Metabolite Behavior After Different Routes of Morphine Administration: Demonstration of the Importance of the Active Metabolite Morphine-6-Glucuronide. *Clin. Pharmacol. Ther.* **1990**, *47*, 12−19.
(70) Glare, P. A.; Walsh, T. D. Clinical Pharmacokinetics of Morphine. *Ther. Drug Monit.* **1991**, *13*, 1−23.
(71) Toll, L.; Berzetei-Gurske, I. P.; Polgar, W. E.; Brandt, S. R.; Adapa, I. D.; Rodriguez, L.; Schwartz, R. W.; Haggart, D.; O'Brien, A.; White, A.; Kennedy, J. M.; Craymer, K.; Farrington, L.; Auh, J. S. Standard Binding and Functional Assays Related to Medications Development Division Testing for Potential Cocaine and Opiate Narcotic Treatment Medications. *NIDA Res. Monogr.* **1998**, *178*, 440−466.
(72) Wentland, M. P.; Ye, Y.; Cioffi, C. L.; Lou, R.; Zhou, Q.; Xu, G.; Duan, W.; Dehnhardt, C. M.; Sun, X.; Cohen, D. J.; Bidlack, J. M. Syntheses and Opioid Receptor Binding Affinities of 8-Amino-2,6-Methano-3-Benzazocines. *J. Med. Chem.* **2003**, *46*, 838−849.
(73) Foye, W. O.; Lemke, T. L.; Williams, D. A. *Foye's Principles of Medicinal Chemistry*, 6th ed.; Lippincott Williams & Wilkins: 2008.
(74) Yamaotsu, N.; Hirono, S.; Nagase, H. 3D-Pharmacophore Identification for Kappa-Opioid Agonists Using Ligand-Based Drug-Design Techniques. *Top. Curr. Chem.* **2011**, *299*, 277−307.
(75) Uhl, G. R.; Childers, S.; Pasternak, G. An Opiate-Receptor Gene Family Reunion. *Trends Neurosci.* **1994**, *17*, 89−93.
(76) Surratt, C. K.; Johnson, P. S.; Moriwaki, A.; Seidleck, B. K.; Blaschak, C. J.; Wang, J. B.; Uhl, G. R. -Mu Opiate Receptor. Charged Transmembrane Domain Amino Acids are Critical for Agonist Recognition and Intrinsic Activity. *J. Biol. Chem.* **1994**, *269*, 20548−20553.
(77) Lavecchia, A.; Greco, G.; Novellino, E.; Vittorio, F.; Ronsisvalle, G. Modeling of Kappa-Opioid Receptor/Agonists Interactions Using Pharmacophore-Based and Docking Simulations. *J. Med. Chem.* **2000**, *43*, 2124−2134.
(78) Berlin, M.; Boyce, C. W.; Ruiz Mde, L. Histamine H3 Receptor as a Drug Discovery Target. *J. Med. Chem.* **2011**, *54*, 26−53.
(79) Corbett, A. D.; Kosterlitz, H. W. Bremazocine is an Agonist at Kappa-Opioid Receptors and an Antagonist at Mu-Opioid Receptors in the Guinea-Pig Myenteric Plexus. *Br. J. Pharmacol.* **1986**, *89*, 245−249.
(80) Tamura, T.; Ogawa, J.; Taniguchi, T.; Waki, I. Preferential Action of Eptazocine, a Novel Analgesic, with Opioid Receptors in Isolated Guinea Pig Ileum and Mouse vas Deferens Preparations. *Folia Pharmacol. Jpn.* **1990**, *95*, 41−46.
(81) Ronsisvalle, G.; Pasquinucci, L.; Pappalardo, M. S.; Vittorio, F.; Fronza, G.; Romagnoli, C.; Pistacchio, E.; Spampinato, S.; Ferri, S. Non-Peptide Ligands for Opioid Receptors. Design of Kappa-Specific Agonists. *J. Med. Chem.* **1993**, *36*, 1860−1865.

DOI: 10.1021/ci500523z
J. Chem. Inf. Model. 2015, 55, 614−627